Exploiting Adaptability in Soft Feet for Sensing Contact Forces

Domenico Mura[1], Cosimo Della Santina[1], Cristina Piazza[1], Irene Frizza[1], Cecilia Morandi[1], Manolo Garabini[1], Giorgio Grioli[2], Manuel G. Catalano[2]

***Abstract*—The large majority of legged robots currently employ ball-feet or flat-feet. More recently soft feet have been introduced, to improve walking performance on uneven grounds. Nevertheless, their novel adaptability requires sensor systems beyond traditional Force/Torque sensors to estimate the distribution of forces on the contact surface. This paper shows how a perception layer realized with Inertial Measurement Units allows a soft foot to reconstruct not only the shape of the foot - hinting at the shape of the ground beneath - but also, under precise hypotheses, the contact force distribution. The problem is theoretically formalized and analysed with a quasi-static approach in the Sagittal plane. Then, theoretical results are experimentally validated in a simplified foot-ground interaction scenario. The force reconstruction provided by the proposed method allows to correctly identify the sole contact location arising from obstacles with radius down to 1 cm.**

***Index Terms*—Natural Machine Motion; Deep Learning in Robotics and Automation; Modeling, Control, and Learning for Soft Robots; Grasping.**

I. Introduction

The locomotion efficiency and effectiveness of living beings is still unparalleled by their robotic counterpart, both in terms of cost of transport, and in the roughness of the terrain that a robot can negotiate if compared to humans.

It is a common conviction in the bio-mechanics field that the merit for these superior abilities is largely to be attributed to the mechanical properties of ankle, sole, and phalanges constituting the human foot [1]. Interestingly, very little research has been conducted so far in foot design for robotic locomotion. Quadrupedal robots often feature feet with cylindrical or spherical shape [2], [3], while the most advanced humanoid robots have flat feet. Examples of different architectures exist, such as flat feet with compliant elements [4], and actuated feet [5].

Manuscript received: June, 8, 2019; Revised September, 16, 2019; Accepted October, 17, 2019. This paper was recommended for publication by Editor Nikolaos G. Tsagarakis upon evaluation of Reviewers' comments. This project has received funding from the European Union under the Horizon 2020 research and innovation program, grant No. 780883 (THING) and by the European Research Council under the Synergy Grant Natural BionicS (No. 810346). The content of this publication is the sole responsibility of the authors. The European Commission or its services cannot be held responsible for any use that may be made of the information it contains.

[1] D. Mura, C. Della Santina, C. Piazza, I. Frizza, C. Morandi and M. Garabini are with the Centro di Ricerca "Enrico Piaggio", Università di Pisa, Largo Lucio Lazzarino 1, 56126 Pisa, Italy {mura.domenico87, cosimodellasantina, irenefrizza, cecilia.morandi, manolo.garabini}@gmail.com

[2] G. Grioli and M. G. Catalano are with the Soft Robotics for Human Cooperation and Rehabilitation, Fondazione Istituto Italiano di Tecnologia, via Morego, 30, 16163 Genova, Italy {giorgio.grioli, manuel.catalano}@gmail.com

We acknowledge Mattia Poggiani and Gaspare Santaera for their help with the experimental setup, and warmly thank Antonio Bicchi for general inspiration and support.

Digital Object Identifier (DOI): see top of this page.

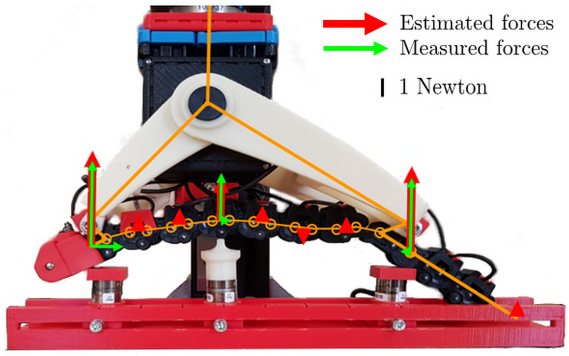

Fig. 1. The reconstruction of the contact forces on a soft robotic foot sole allowed by the proposed method. Three 6 axis F/T sensors are placed in contact with the robotic foot metacarpus, heel and plantar fascia, and their measured force is visualized in green. The estimated forces on the foot sole, shown in red, is estimated by the foot pose reconstruction filtering process, allowed by IMU sensorization.

More recently, several novel adaptive feet designs have been proposed [6], [7], [8], [9]. Based on the so-called soft robotics paradigm, they feature high-compliance elements embedded in the joints and/or in the whole structure. Thanks to the intelligence embodied in their deformable mechanics, this new generation of feet promises to bring robotic locomotion to a higher level of efficiency and robustness. These systems are able to adapt their shape to the environment, strongly reducing slippage and interaction instability on unknown and uneven terrain w.r.t ball-feet and flat-feet. For the systems equipped with ball-feet and flat-feet the most common sensing approach is the adoption of force-torque (F/T) sensors, which enable to reconstruct the global wrench caused by the foot-ground interaction. Similarly to general external contact localization algorithms, of which one recent example is presented in [10], state of the art locomotion algorithms exploit force and torque measurements to reactively plan and control the robot motion, by heavily relying on strong assumptions. In case of ball-feet the foot-ground contact is supposed to happen through a point [11], and in case of flat-feet the contact surface is often assumed to coincide with the complete foot sole [12]. These oversimplifying hypotheses are necessary because the commonly adopted sensing systems do not allow to know the contact surface, nor the force distribution under the foot sole. Attempts to equip feet with sensor matrices [13] still pose a major challenge, because the large shear forces easily damage them. To provide flexible link robots with a perception system is a challenging task, not yet explored for adaptive feet, given the novelty of their concepts. Relatively more work exists instead for sensing with soft hands, e.g. in [14] authors consider the problem of deriving tactile data solely from proprioceptive sensors attached to the actuator of a single under-actuated finger. In [15] we proved that

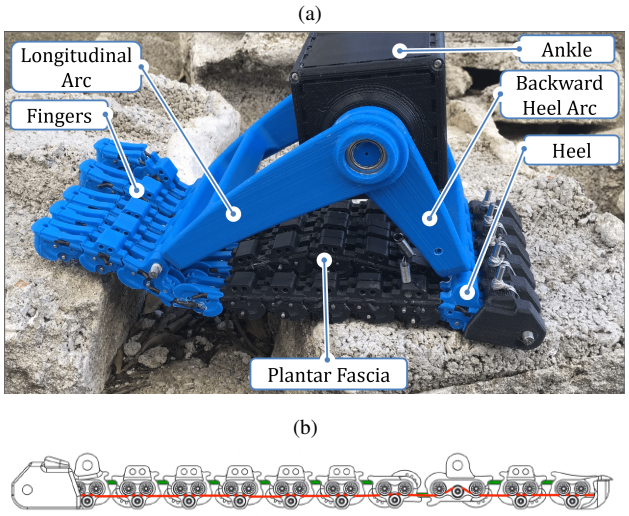

Fig. 2. a) Prototype of the SoftFoot, with highlighted body segments, while interacting with an irregular terrain. b) CAD of the SoftFoot sole, with elastic ligaments in green and tendon in red.

accurate force sensing can be achieved from only postural information, when a model of hand compliance is available. In this work we tackle for the first time the problem of estimating contact forces in soft feet from purely postural measurements, by exploiting the intrinsic capability of these systems to conform to the environment. More specifically, we propose a perception system that relies on Inertial Measurements Units (IMUs) placed on top of the adaptive foot links, as the only source of direct measurements. First, we show that this perception system enables the accurate reconstruction of the foot posture (as shown in Fig. 1). We then introduce an algorithm that estimates the contact points of the foot sole and the force distribution under the contact surface - based on the IMU measurements and on the foot quasi-static model. The algorithm is specifically tailored on the SoftFoot - introduced in [6] - but its working principles are generally applicable to a vast kind of soft feet. Thanks to the freedom in the placement of the IMUs, the solution we propose does not suffer from the drawbacks given by the direct contact of the sensing parts with the environment. Finally, we present a first experimental validation of our method in a simplified interaction scenario.

II. Motivation

The human foot is a very compliant system [16]. Its rigid structure is highly articulated, thus implementing a good trade-off between softness and strength. A complete description of all the possible interaction phenomena which happen during a walking gait is a very complex and faceted task. The contact, in general, will be characterized by a very complex distribution of forces, possibly accounting for a mixture of static and dynamic friction conditions, depending on the relative slip between the different tangent surfaces.

Although to walk is a fairly complex dynamic process, among the walking phases a quasi-static phase exists. The quasi-static phase of the foot-ground interaction is of paramount importance, because it is during this phase that a consistent part of the equilibrium control of a biped is performed. Indeed, a very useful, at times fundamental, information required to implement equilibrium control is the determination of the distribution of contact forces between the foot and the soil, as discussed in detail in [6].

During the quasi-static phase, when a successful and stable foothold acquisition arises, the foot achieves a quasi-static equilibrium, during which both the foot and the soil do not substantially move. In this phase a slow change in the loading conditions can be observed, corresponding to e.g. the small balancing corrections that a biped operates to preserve the upright equilibrium [17], or to the load transfer typical of the mid-stance phase of a walking stride [18].

This paper tackles the problem of identifying the contact force distributions of a soft foot interacting with an irregular ground during a quasi-static phase. For the sake of simplicity, we restrict the analysis to the two-dimensional problem that arises when constraining the phenomenon to the Sagittal plane (as this simplified analysis accounts for a non-negligible fragment of the whole phenomenon).

In this work, the proposed method and the consequent experimental validation are applied to the architecture of the SoftFoot, shown in Fig. 2, which was introduced in [6] for applications in both robotics and prosthetics. This system presents a highly articulated soft architecture aiming at reproducing the main characteristics of a human foot. The SoftFoot is a completely passive system, which varies its shape and stiffness in function of the exerted forces, through a system of pulley, tendons and springs placed in the structure. Although here we explicitly consider the SoftFoot system, the possibility to apply the approach to different kind of feet with different soft architectures is still possible.

TABLE I
Equations and Variables of the Foot Model

	Origin	N. of Variables
Foot Part	Long. Arc	$2+2+2$
	Plantar Fascia	$3(2n_p+2)$
	Toe Phalanges	$3(2n_t)$
Force	Heel Contact Force	3
	Fascia Contact Force	$3n_p$
	Met. Contact Force	3
	Toe Contact Force	$3n_t$
	Tendon Force	1

	Origin	N. of Equations
Equilibria	Long. Arc	$3(2+2)$
	Plantar Fascia	$3(2n_p+1)$
	Toe Phalanges	$3(2n_t)$
Torque Constraints	Heel Contact Force	3
	Fascia Contact Force	n_p+1
	Toe Contact Force	n_t

III. Estimating Interaction Forces from Posture Informations

A. A complete model of the foot

As shown in Fig. 3(b), the SoftFoot can be divided into four rigid bodies and two articulated subsystems. We hypothesize in the following negligible segment masses in the foot. This is typically true in the practice, and it is an hypothesis often introduced in robotic hands [19]. As a result, mass-related

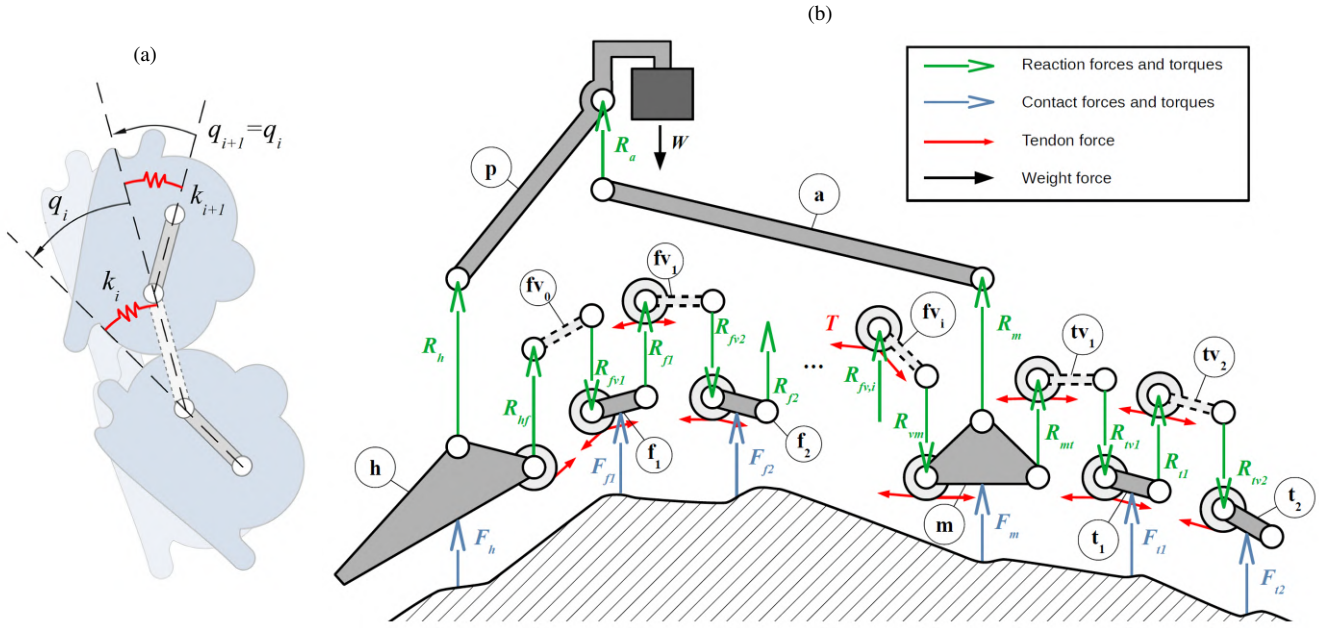

Fig. 3. Foot model. a) Model of a plantar fascia/toe finger phalanx. Each pair of modules is modelled as a system of three bodies, two physical ones corresponding to the two modules and a virtual link connecting the two through two revolute joints. In nominal working condition a geared profile engages the two modules, constraining the relative rotations between each of the two and the virtual link (q_i and q_{i+1}) to be symmetric. An elastic ligament (not shown in figure) acts on the pair of modules and is represented by the two springs of stiffness k. b) Free-body diagram of the SoftFoot interacting with the ground. The bodies that compose the foot are in dark gray, the virtual links are in light gray and the concentrated system mass is in deep dark grey. The internal sets of reaction forces/torques exchanged by the bodies and the sets of contact forces and torques are in green and blue, respectively. The tension force of the tendon is shown in red and the weight force in black. Forces and torques enter with a positive contribution in the equilibrium equations when the arrows point toward the object and with a negative contribution otherwise. Full triangular point arrows indicate simple forces, while outlined sharp-point arrows indicate that the two bodies united by the arrows exchange a two-dimensional force and one torque. Thus, W and T are scalar variables that represent the signed modulus of the corresponding vector in figure, while the $F_{(.)}$ and $R_{(.)}$ are vector quantities.

forces internal to the foot will be neglected, and the whole robot mass W considered concentrated above the ankle (as shown with deep dark grey in Fig. 3(b)). The four bodies are the backward heel arc p, the frontal arch/ankle a, the heel h, and the metacarpus m. The two articulated subsystems are the plantar fascia - or simply fascia - and the (toe) finger. In the SoftFoot, the fascia and the fingers are composed of a series of modular components, first introduced as phalanges of the Pisa/IIT SoftHand [20]. Such elements are kept together by a set of two elastic ligaments for each coupling, and are designed to roll on each other by relying on a particular flexible implementation of the Rolamite joint [21]. A series of n of these links can be modelled by a chain of $2n-1$ links, coupled by $2n-2$ revolute joints. n of these links correspond to the real ones, while the other $n-1$ constitute a set of equivalent virtual joints that keep a fixed distance between the two rolling surface centres (see [19] for details). The Rolamite joint modelling adopted here is shown in Fig. 3(a).

We call n_t the number of modules used in the finger. Here, rigid links $t_1 \dots t_{nt}$ are connected between them and to the metacarpus by n_t virtual links $t_{\mathrm{v}1} \dots t_{\mathrm{v}n_t}$, forming an open chain. The fascia is very similar, with the only difference that it connects on both the heel and the metacarpus - producing a closed chain - yielding n_p rigid links $f_1 \dots f_{n_p}$ connected between them and to the heel/metacarpus by n_p+1 virtual bodies $f_{\mathrm{v}0} \dots f_{\mathrm{v}n_p}$. These modular elements are all coupled by a tendon with negligible elasticity that routes through a series of idle pulleys mounted on the modules, with their axles aligned with the center of the rolling surfaces. All the modules of both the finger and the fascia are coupled by the same tendon which routes also through the metacarpus and up to heel bone. In Fig. 3(b), the reaction forces between the different segments are represented in green, the terrain contact forces in blue and the tendon force T in red. We can not report here the full model for the sake of space, but we will report later in the text the equations that we use to derive the here proposed algorithm. Although in our analysis we pose ourselves in a quasi-static setup, we remark that the quasi-static hypothesis can be swiftly removed, so to allow also dynamic considerations in future extensions of this work. Indeed, the discrepancies in the foot segment model equations would be negligible, as the foot body masses are very small. Regarding the only non-negligible system mass, i.e the robot mass which accounts for the weight W in Fig. 3(b), we would most likely know the mass acceleration of the robot leg to be connected to the foot [1], i.e. the inertial force to add to the equations.

B. A first attempt at reducing the number of unknowns

The complete model proposed in the previous section leads to a problem where the number of variables $(19+9(n_P+n_T))$, is larger than the number of equations $(16+7(n_P+n_T))$, and even larger than the number of non redundant equations $(14+7(n_P+n_T)$, closing the chain through a revolute joint makes two of the equations redundant). This is detailed in

Tab. I. In other terms, there are infinite choices of internal and external forces that can produce a same configuration of the foot. This represents a drawback of our setup, as it could introduce errors in the estimation of the contact force distribution that can, in turn, perturbate the stability of walking. We try to overcome this ambiguity as follows. A solution consists in adding further relations by taking into account a model of the terrain. However, it is not reasonable to have available such a model, since it is the very final goal of our analysis to identify it by means of the interactions with the foot. As an alternative, we propose here to introduce further assumptions on the nature of the interactions with the environment, which could in turn be translated into simplified equations. A straightforward choice could be to employ the same assumptions used for the grasping problem as introduced in [15]

a) H_0-1: : The friction cone (of the contact between foot and ground) is very small, i.e. tangential forces are negligible. This is a strong hypothesis for the locomotion case. However it seems reasonable for a foot interacting with the ground mainly along the vertical direction, as we suppose here. The number of variables is reduced by $2 + (n_P + n_T)$.

b) H_0-2: : The contact force is acting in the middle of the maximum contact area of each element. This hypothesis reduces the variable number by $2+(n_P+n_T)$, as we remove the torque components from the interaction wrenches.

These assumptions together allows to remove $4 + 2(n_P + n_T)$ variables from the problem - leading to $14+7(n_P+n_T)$ equations in $15 + 7(n_P + n_T)$ variables. One can now see that one variable is still left over. Following along this line would thus require introducing another assumption on either the internal or external forces. This is not straightforward to be conceived. We thus have to follow a different path.

C. Novel set of assumptions producing a square system

To build the novel set of assumptions, we look for another set of hypotheses specifically tailored on our problem. In particular, we consider that to employ the Rolamite joints for the SoftFoot fascia and fingers entails that their phalanges can become highly dislocated during interaction. The phalanges are likely to lose contact between each other, while remaining connected only by the action of the tendon and the spring. In our case this can be translated in neglecting the transmission of torques, which would have been mediated by the gears which are no more in contact. Thus, the novel set of hypotheses results

a) H-1: Same as H_0-1. This hypothesis reduces the number of variables by $2 + (n_P + n_T)$.

b) H-2: The contact torques between the phalanges are negligible, when not null. This hypothesis reduces the number of variables by $2 + 2(n_P + n_T)$, while also reducing the amount of equations by $1 + (n_P + n_T)$.

c) H-3: The contact on the last phalanx of the finger happens on the tip, and the point of contact on the two triangular bodies is the center of the whole contact area. This hypothesis reduces the number of variables by 3.

By applying H-1 $-$ H-3 we obtain a square system were the variables are $14 + 6(n_P + n_T)$ as the independent equations. Within this condition, we list now the equations for each rigid body. Please refer to Fig. 3(a) for the body and force notation, and to Tab. II for the notation of (scalar) quantities employed in the foot model equations.

TABLE II
NOTATION FOR FOOT MODEL

Symbol	Definition
$R_{\mathrm{r,c}}$	Component along $\mathrm{c} \in \{\mathrm{x},\mathrm{y}\}$ of reaction force $\mathrm{r} \in \{\mathrm{a},\mathrm{h},\mathrm{m}\}$
$R_{\mathrm{f}i,\mathrm{c}}$	Component along $\mathrm{c} \in \{\mathrm{x},\mathrm{y}\}$ of the reaction force between bodies f_i and $f_{\mathrm{v}i}$, $i \in \{1,\dots n_p\}$
$R_{\mathrm{fv}i,\mathrm{c}}$	Component along $\mathrm{c} \in \{\mathrm{x},\mathrm{y}\}$ of the reaction force between body $f_{\mathrm{v}i-1}$ and f_i, $i \in \{1,\dots n_p\}$
$R_{\mathrm{t}i,\mathrm{c}}$	Component along $\mathrm{c} \in \{\mathrm{x},\mathrm{y}\}$ of the reaction force between bodies t_i and $t_{\mathrm{v}i}$, $i \in \{1,\dots n_t\}$
$R_{\mathrm{tv}i,\mathrm{c}}$	Component along $\mathrm{c} \in \{\mathrm{x},\mathrm{y}\}$ of the reaction force between body $t_{\mathrm{v}i-1}$ and t_i, $i \in \{1,\dots n_t\}$
$R_{\mathrm{hf,c}}$	Component along $\mathrm{c} \in \{\mathrm{x},\mathrm{y}\}$ of the reaction force between body h and $f_{\mathrm{v}0}$
$R_{\mathrm{vm,c}}$	Component along $\mathrm{c} \in \{\mathrm{x},\mathrm{y}\}$ of the reaction force between body $f_{\mathrm{v}2n_p}$ and m
$R_{\mathrm{mv,c}}$	Component along $\mathrm{c} \in \{\mathrm{x},\mathrm{y}\}$ of the reaction force between body m and $t_{\mathrm{v}1}$
W	weight of the robot
T	tendon pulling force
$F_{\mathrm{h}}, F_{\mathrm{m}}$	(vertical) contact force of body h / m
$F_{\mathrm{f}i}$	(vertical) contact force of body f_i, $i \in \{1,\dots n_p\}$
$F_{\mathrm{t}i}$	(vertical) contact force of body t_i, $i \in \{1,\dots n_t\}$
r	pulley radius
b_W	lever of W w.r.t. the joint connecting p to h
L_{b}	length of body $\mathrm{b} \in \{\mathrm{a},\mathrm{p},\mathrm{t}\}$
α_{b}	angle of body $\mathrm{b} \in \{\mathrm{a},\mathrm{p},\mathrm{t}\}$
$\beta_{\mathrm{h}}, \beta_{\mathrm{m}}$	angle of body h / m
β_i	angle of $i-$th plantar fascia body, $i \in \{1,\dots 2n_p+1\}$
$\beta_{\mathrm{t},i}$	angle of $i-$th toe finger body, $i \in \{1,\dots 2n_t+2\}$
x_i, y_i	coordinates of the fascia $i-$th joint axis, $i \in \{1,\dots 2n_p\}$
x_{h}, y_{h}	coordinates of axis of the joint connecting bodies h and $f_{\mathrm{v}0}$
$\tau_{\mathrm{k},i}$	pulley spring elastic torque, $i \in \{1,\dots 2(n_p+n_t)+1\}$

Imposing the equilibrium of forces (first two rows) and moments (third row) for body p and a yields

$$\begin{bmatrix} 1 & 0 & 1 & 0 \\ 0 & 1 & 0 & 1 \\ 0 & 0 & -L_a \mathrm{s}_{\alpha_p} & L_a \mathrm{c}_{\alpha_p} \end{bmatrix} \begin{bmatrix} R_{\mathrm{h,x}} \\ R_{\mathrm{h,y}} \\ R_{\mathrm{a,x}} \\ R_{\mathrm{a,y}} \end{bmatrix} = \begin{bmatrix} 0 \\ W \\ b_W W \end{bmatrix}, \quad (1)$$

$$\begin{bmatrix} 1 & 0 & 1 & 0 \\ 0 & 1 & 0 & 1 \\ 0 & 0 & -L_{\mathrm{p}} \mathrm{s}_{\alpha_a} & L_{\mathrm{p}} \mathrm{c}_{\alpha_a} \end{bmatrix} \begin{bmatrix} R_{\mathrm{a,x}} \\ R_{\mathrm{a,y}} \\ R_{\mathrm{m,x}} \\ R_{\mathrm{m,y}} \end{bmatrix} = \begin{bmatrix} 0 \\ 0 \\ 0 \end{bmatrix}, \quad (2)$$

where c_θ and s_θ denote, from now on, the sine and cosine of an angle θ, respectively.

The equilibrium at body h comprises also the tendon pulling force T, and the environment interaction F_{h}

$$\begin{bmatrix} 0 & c_{\beta_1} - c_{\beta_{\mathrm{h}}} & 1 & 0 & -1 & 0 \\ 1 & s_{\beta_1} - s_{\beta_{\mathrm{h}}} & 0 & 1 & 0 & -1 \\ 0 & e_{\mathrm{h}}(\beta_{\mathrm{h}}, \beta_1) & d_{\mathrm{h}} & -n_{\mathrm{h}} & b_{\mathrm{h}} s(\beta_{\mathrm{h}}) & b_{\mathrm{h}} c_{\beta_{\mathrm{h}}} \end{bmatrix} \begin{bmatrix} F_{\mathrm{h}} \\ T \\ R_{\mathrm{h,x}} \\ R_{\mathrm{h,y}} \\ R_{\mathrm{hf,x}} \\ R_{\mathrm{hf,y}} \end{bmatrix} = \begin{bmatrix} 0 \\ 0 \\ \tau_{\mathrm{k},1} \end{bmatrix}, \quad (3)$$

where $e_{\mathrm{h}}(\beta_{\mathrm{h}}, \beta_1)$, d_{h}, n_{h} and b_{h} are geometrical quantities (which we do not report here for the sake of space) that serve as levers from the forces and the moment pole. $\tau_{\mathrm{k},1}$ is the elastic torque due to the torsional spring present in the pulley incorporated in the body. Body m equilibrium is similar to

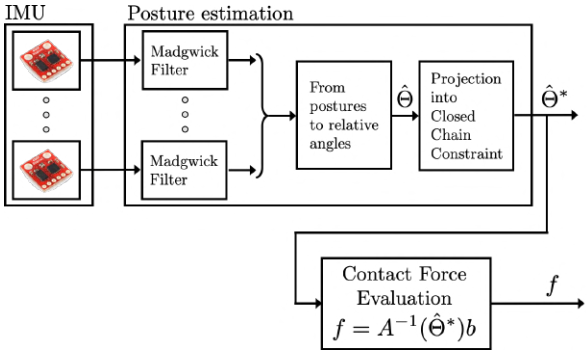

Fig. 4. Complete architecture of the proposed method. Its main components are: i) extraction of the full posture of the foot from the IMU measurements and the Madgwick filter, ii) merging of the posture reconstruction with the *a priori* knowledge of the model, and iii) reconstruction of the contact force set by means of the kinematic regression allowed by the model structure.

the one of body h

$$\begin{bmatrix} c_{\beta_{2n_p}} & 1 & 0 & 1 & 0 & -1 & 0 & 0 \\ s_{\beta_{2n_p}} & 0 & 1 & 0 & 1 & 0 & -1 & 1 \\ 0 & e_{\mathrm{m}}(\beta_{\mathrm{m}}) & d_{\mathrm{m}}(\beta_{\mathrm{m}}) & -b_{\mathrm{m}}s_{\beta_{\mathrm{m}}} & n_{\mathrm{m}}c_{\beta_{\mathrm{m}}} & 0 & 0 & n_{\mathrm{m}}c(\beta_{\mathrm{m}}) \end{bmatrix} \begin{bmatrix} T \\ R_{\mathrm{m,x}} \\ R_{\mathrm{m,y}} \\ R_{\mathrm{mt,x}} \\ R_{\mathrm{mt,y}} \\ R_{\mathrm{fv}2n_p,\mathrm{x}} \\ R_{\mathrm{fv}2n_p,\mathrm{y}} \\ F_{\mathrm{m}} \end{bmatrix} = \begin{bmatrix} 0 \\ 0 \\ \tau_{\mathrm{k},2n_p+2} - \tau_{\mathrm{k},2n_p+1} \end{bmatrix}, \tag{4}$$

where $e_{\mathrm{m}}(\beta_{\mathrm{m}})$, $d_{\mathrm{m}}(\beta_{\mathrm{m}})$, b_{m} and n_{m} are geometrical quantities representing the levers of forces w.r.t. the moment pole. The equations related to each body $f_1 \dots f_{n_p}$ and $f_{\mathrm{v}1} \dots f_{\mathrm{v}n_p}$ are similar and results in the form (here for a generic body f_i)

$$\begin{bmatrix} 0 & \Delta_{\mathrm{c}i} & -1 & 0 & 1 & 0 \\ 1 & \Delta_{\mathrm{s}i} & 0 & 1 & 0 & -1 \\ 0 & 0 & 0 & 0 & \Delta_{\mathrm{x}i} & \Delta_{\mathrm{y}i} \end{bmatrix} \begin{bmatrix} F_{\mathrm{f}i} \\ T \\ R_{fi,\mathrm{x}} \\ R_{fi,\mathrm{y}} \\ R_{\mathrm{fv}i,\mathrm{x}} \\ R_{\mathrm{fv}i,\mathrm{y}} \end{bmatrix} = \begin{bmatrix} 0 \\ 0 \\ \tau_{\mathrm{k},2} - \tau_{\mathrm{k},1} \end{bmatrix}, \tag{5}$$

where $\Delta_{\mathrm{c}i} = c_{\beta_{2i}} - c_{\beta_{2i-1}}$ (similar definition for $\Delta_{\mathrm{s}i}$) and $\Delta_{\mathrm{x}i} = x_i - x_{i+1}$ (similar definition for $\Delta_{\mathrm{y}i}$).
Body $f_{\mathrm{v}0}$ slightly differs from the other bodies of the fascia since it has no tendon force acting on it (see Fig. 3(a))

$$\begin{bmatrix} 1 & 0 & -1 & 0 \\ 0 & 1 & 0 & -1 \\ 0 & 0 & -x_1 + x_{\mathrm{h}} & y_1 - y_{\mathrm{h}} \end{bmatrix} \begin{bmatrix} R_{\mathrm{hf,x}} \\ R_{\mathrm{hf,y}} \\ R_{\mathrm{fv}1,\mathrm{x}} \\ R_{\mathrm{fv}1,\mathrm{y}} \end{bmatrix} = \begin{bmatrix} 0 \\ 0 \\ \tau_{\mathrm{k},2} - \tau_{\mathrm{k},1} \end{bmatrix}. \tag{6}$$

Finally, the generic bodies t_i and $t_{\mathrm{v}i}$ - representing phalanges of the finger - have the same structure of f_i and $f_{\mathrm{v}i}$, with the exception of the last phalanx being

$$\begin{bmatrix} 0 & -c_{\beta_{\mathrm{t},2n_t+2}} & -1 & 0 \\ 1 & -s - \beta_{\mathrm{t},2n_t+2} & 0 & -1 \\ L_{\mathrm{t}} & -r & 0 & 0 \end{bmatrix} \begin{bmatrix} F_{\mathrm{t}} \\ T \\ R_{\mathrm{t},2n_t+1,\mathrm{x}} \\ R_{\mathrm{t},2n_t+1,\mathrm{y}} \end{bmatrix} = \begin{bmatrix} 0 \\ 0 \\ \tau_{\mathrm{k},2(n_p+n_t)+1} \end{bmatrix}, \tag{7}$$

where F_{t} is the contact force applied at the tip.

D. Evaluation of forces

The matrix subsystems of previous section can be arranged in a square matrix A to represent the whole system with the general form $A(\Theta)f = b(\Theta)$, where f is the vector of internal and external forces, b is the collection vector of all known quantities, and Θ is the entire foot posture vector - which sensing and estimation we will describe in the next section. In particular, Θ contains the orientation of all the phalanges $\beta_{ti}, i = 1 \dots 2n_t + 1$, $\beta_i, i = 1 \dots 2n_p + 1$ and the orientation of the other four bodies β_{m}, β_{h}, α_{p}, α_{a}.

It is worth underlining that in our implementation b contains linear elastic forces and a specific model of the weight of the robot. However, more complex models of these effects can be easily integrated - e.g. a nonlinear elastic field, the whole robot configuration-dependent weight distribution - without modifying the structure introduced above. The global system matrix A is partitioned as

$$\begin{array}{r} \text{Body p} \\ \text{Body h} \\ \text{First P.F. Body} \\ \text{P.F. Bodies} \\ \text{Body m} \\ \text{Body t} \end{array} \left\{ \begin{bmatrix} A_{\mathrm{p,F}} & A_{\mathrm{p,T}} & A_{\mathrm{p,R}} \\ A_{\mathrm{m,F}} & A_{\mathrm{m,T}} & A_{\mathrm{m,R}} \\ A_{\mathrm{fv0,F}} & A_{\mathrm{fv0,T}} & A_{\mathrm{fv0,R}} \\ A_{\mathrm{f,F}} & A_{\mathrm{f,T}} & A_{\mathrm{f,R}} \\ A_{\mathrm{m,F}} & A_{\mathrm{m,T}} & A_{\mathrm{m,R}} \\ A_{\mathrm{t,F}} & A_{\mathrm{t,T}} & A_{\mathrm{t,R}} \end{bmatrix} \right., \quad \begin{array}{ccc} \underbrace{} & \underbrace{} & \underbrace{} \\ \text{Contact} & \text{Tension} & \text{Reaction} \end{array} \tag{8}$$

where the sub matrix $A_{\mathrm{i,J}}$ refers to the foot segment i subject to the force type J (same notation as in Fig. 3). The unknown forces are thus arranged in the vector f

$$f = [\ f_{\mathrm{F}}^T \mid T \mid f_{\mathrm{R}}^T\ ]^T, \tag{9}$$

where f_{F} collects the contact forces, T is the tendon tension, and f_{R} collects all the reaction forces between the foot body parts. The matrix A has full rank, so it is possible to define its inverse and to obtain an estimation of the forces contained in the vector f by setting

$$f = A^{-1}(\Theta)b(\Theta), \tag{10}$$

which will be our estimator of internal and external forces, and it correctly depends only on the configuration vector Θ.

IV. General Architecture

The proposed framework is shown in Fig. 4, and it is composed by two main components. The first extracts the full posture of the foot from the IMU measurements. This information is merged by the second layer with the *a priori* knowledge of the model, to estimate a set of contact forces by means of the kinematic regression allowed by the model structure. This second layer was introduced in the previous section, while the first layer will be introduced here.

In continuity with [15], a Madgwick filter is used to extract posture information from each IMU. An estimation of the angles $\hat{\Theta}$ is then obtained by simple projection of the 3D rigid body rotation to the plane on which the joints move. To cope with the lack of magnetometer measurements and with the noise associated to the accelerometer readings, we exploit the closed chain constraint imposed by the kinematics of the foot, refining the estimation. This is instrumental in

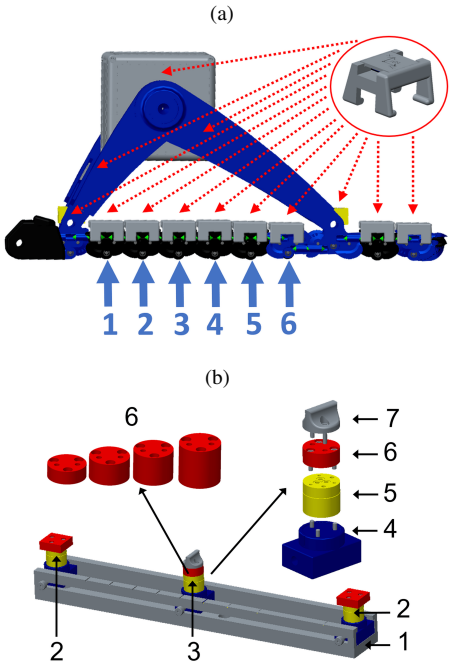

Fig. 5. Fig. 4(a) shows the chain of modules that constitute the fascia and the finger of the SoftFoot. The locations of the IMUs (mounted on a support) are highlighted. Fig. 4(b) shows the linear guide (1) used to place both the fixed obstacles (2) and the sliding obstacle (3). The obstacles are composed of the following parts: i) a F/T sensor (5), placed in a custom-made support (4); ii) a support (6) where the contact with the foot occurs in the fixed obstacles, and that is of different heights in the sliding obstacle; and iii) an apical rubber part (7) for the sliding obstacle.

our aim to substitute F/T sensors with our method, as one of the shortcomings of IMU sensorization w.r.t. to force sensing is the noisiness of acceleration sensing. Knowing the relative angle estimates it is possible to calculate the value of the length of body a - namely $\hat{l}_\mathrm{a}$ - as

$$\begin{aligned} \hat{l}_\mathrm{a} c_{\hat{\alpha}_\mathrm{a}} + l_\mathrm{p} c_{\hat{\alpha}_\mathrm{p}} &= L(\hat{\beta}_\mathrm{h}, \hat{\beta}_1, \dots \hat{\beta}_{2np+1}, \hat{\beta}_\mathrm{m}) \\ \Rightarrow \hat{l}_\mathrm{a}(\hat{\Theta}) &= \frac{L(\hat{\beta}_\mathrm{h}, \hat{\beta}_1, \dots \hat{\beta}_{2np+1}, \hat{\beta}_\mathrm{m}) - l_\mathrm{p} c_{\hat{\alpha}_\mathrm{p}}}{c_{\hat{\alpha}_\mathrm{a}}}, \end{aligned} \tag{11}$$

where L is the horizontal component of the distance between the joint connecting h with p and the joint connecting m with a - evaluated as direct kinematics of the serial chain composed by h, m, f_i and $f_{\mathrm{v}i}$. l_p is the length of the body p. The left hand side of the first equation is the explicit form of the same quantity, expressed as direct kinematics of the open chain made of the two bodies p and a. Due to the closed chain constraint the two values must be equal. However, the actual value of l_a is known from the real physical system. Using this information we can reduce the estimation error in the direction of the constraint. We employ the gradient method for locally solving the optimization problem

$$\hat{\Theta}^* = \arg\min_{\Theta} \quad ||\Theta - \Theta^*||^2 + ||\hat{l}_\mathrm{a}(\Theta) - l_\mathrm{a}||^2. \tag{12}$$

After this process, we obtain a new set of angle estimates $\hat{\Theta}^\star$, which will be used to populate the matrix A and the vector b so to reconstruct the force vector $\hat{f}$.

V. Experimental validation

We carried experimental validation to test the accuracy of the force vector reconstruction obtained as described in the previous Section. The complete experimental setup is shown in Fig. 5. The experimental validation goals are i) to observe how close the forces measured by a given number of six-axis F/T sensors placed under the foot sole are to the forces given by the model, and ii) to assess the precision of the proposed method in correctly identifying the application point of a contact force on the foot fascia.

A. Experimental setup

We adapted the SoftFoot in order to have only a single phalanx chain for the fascia and the fingers, see Fig. 4(a). Each phalanx was equipped with an IMU by means of a support, highlighted in Fig. 4(a). Further IMUs were placed in correspondence of the foot arcs to obtain their relative positions. Thus, we employed a total of 13 IMUs (2 for the finger, 6 for the fascia and 5 for the foot arcs) during the experimental validation. The electronic boards for data acquisition and sensing were based on a Cypress PSoC microcontroller and realized under the Natural Machine Motion Initiative[1] framework [20].

We also designed three sensorized "obstacles" to mimic the uneven ground contact points, as reported in Fig. 4(b). Each obstacle is equipped with a six-axis F/T sensor. The obstacles were arranged on an horizontal guide (1), also shown in Fig. 4(b). Two obstacles were fixed at the extremities of the support (2), while a third obstacle (3) was able to slide between different prescribed positions.

The experiment consisted in placing the single-chain SoftFoot sole vertically on the obstacles, getting the obstacle F/T sensor readings and performing the contact force reconstruction via the proposed framework. The foot was placed so that three body segments made a point contact during the experiments, i.e. the heel (body h), the metacarpus (body m) and a single fascia phalanx in contact with the sliding obstacle apical part (body p). Repeatability of measures was ensured by means of a vertical guide, mounted on a frame structure, responsible for the foot vertical motion.
The foot contact locations on the heel and metacarpus were maintained constant during the experimentation. On the contrary, we considered six different positions on the obstacle guide for placing the sliding obstacle (as in the SoftFoot design employed here the fascia is composed of six phalanges, see Fig. 4(a)), so to assess how the force reconstruction process performs along the fascia. To be consistent with our foot model, these positions where in correspondence with the center of each fascia phalanx, as indicated by the blue arrows in Fig. 4(a). The sliding obstacle height was variable thanks to four different custom-made cylindrical supports, so to observe in a simplified case if and how much the (simulated) shape of the ground affects the force reconstruction process. The cylindrical support heights were set as 7 mm, 11 mm, 15 mm and 19 mm. Experiments were performed for each sliding obstacle position and height.

[1] www.naturalmachinemotioninitiative.com

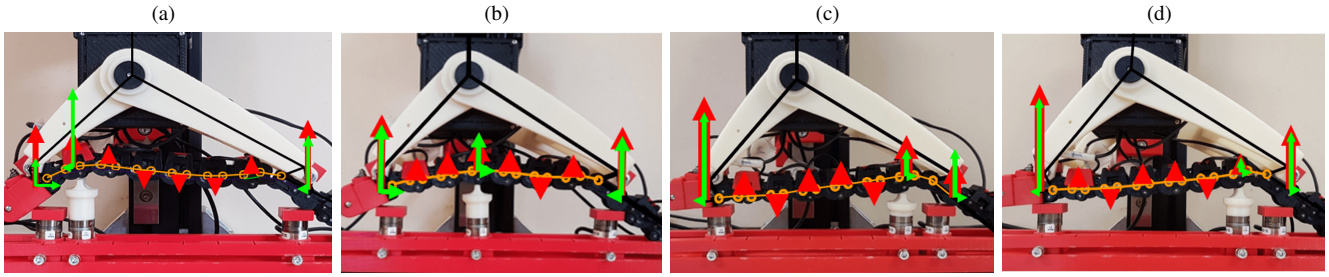

Fig. 6. Figure shows the reconstructed posture of the foot sole in orange, the measured forces in green, and the estimated forces in red. Different positions/heights of the sliding obstacle are shown: a) pos. 2, height 19 mm; b) pos. 3, height 15 mm; c) pos. 6, height 7 mm; d) pos. 6, height 11 mm.

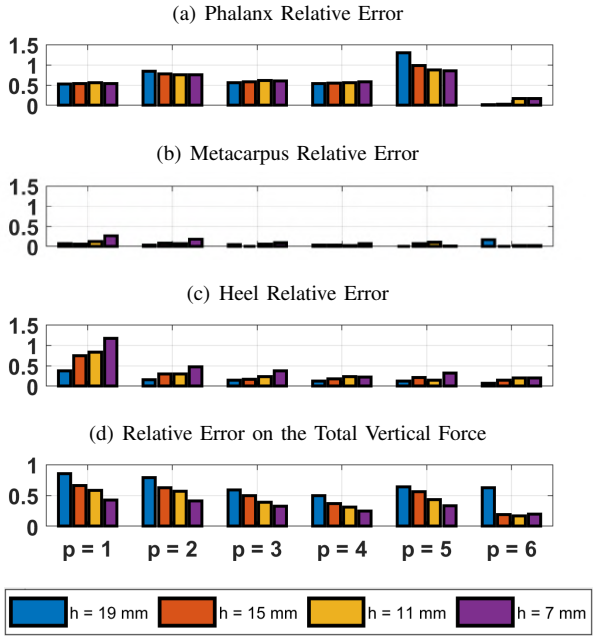

Fig. 7. Experiment results. Figure shows relative errors for three body segments (heel, metacarpus and fascia phalanx in contact with the sliding obstacle), along with the relative error on the total vertical force, for the four sliding obstacle heights h and for its six prescribed positions p along the fascia. The normal force applied on the foot was $\simeq$ 12 N.

The forces obtained by the F/T sensors were used as the ground truth and compared with the forces reconstructed from the general architecture. Therefore, relative errors on the forces were computed for the three body segment. In particular, for the foot segment $\mathrm{b} \in \{\mathrm{p}, \mathrm{m}, \mathrm{h}\}$, the relative (vertical) error was defined as

$$\mathrm{e_b} = (\hat{f}_\mathrm{b} - \tilde{f}_\mathrm{b})/\tilde{f}_\mathrm{b}, \tag{13}$$

where $\hat{f}_\mathrm{b}$ and $\tilde{f}_\mathrm{b}$ are the corresponding estimated force (obtained as shown in Subsec. IV) and the measured force. The relative error on the total vertical force was also computed. It was defined as

$$\mathrm{e_T} = \left[\sum_{i=1}^{3}(\hat{f}_\mathrm{i} - \tilde{f}_\mathrm{i})\right] / \left[\sum_{i=1}^{3}\tilde{f}_\mathrm{i}\right]. \tag{14}$$

During the experiments, the total normal force applied on the foot (i.e. $\sum_{i=1}^{3}\tilde{f}_\mathrm{i}$) was $\simeq$ 12 N. Finally, we aim to assess the precision of the proposed method in correctly identify the application point of a plantar arc contact force. Thus, after performing each iteration of the experiment as described above, we reconstruct and analyse the forces $F_{\mathrm{f1}} \dots F_{\mathrm{f}np}$ for every fascia body. Specifically, we check if the $F_{\mathrm{f}i}$ with higher magnitude corresponds to the phalanx that actually made contact with the sliding obstacle. We did several repetitions of the experiment to increase the result data set and to define a confusion matrix on it. We performed 8 repetitions for each sliding obstacle position. In every position case each obstacle height was presented two times.

B. Experimental results

Figs. 1 and 6 show the concept of the experiment results, visualizing the forces estimated by the model in red and the forces measured by the sensors in green, for different positions and heights of the plantar obstacle support. The contact horizontal forces are plotted only in green, as we have modelled them as purely vertical in the foot model. The reconstructed foot sole posture is also shown in orange.

Fig. 7 shows the relative errors for the three body segments recalled in the previous Subsection (heel, metacarpus and plantar arc phalanx in contact with the obstacle), along with the relative error on the total vertical force, for the four sliding obstacle heights and for its six prescribed positions along the fascia. We see that, as the plantar obstacle height increases, $\mathrm{e_T}$ increases for all body segments. Moreover, proceeding for obstacle position from the heel to the metacarpus, the error decreases first, but on phalanx 5 an error peak is present. This is due to the greater angle on the last fascia phalanx which causes a greater estimated force. Thus, when there is an obstacle near it, the error increases.

The confusion matrix from the experimental results is reported in Tab. III. The best results occur when the obstacle is placed on the phalanges 1, 3, 4 and 6, while the identification fails when the contact occurs on phalanges 2 and 5. This appears to be consistent with the results of Fig. 7 for the obstacle position 5. Regarding position 2 one can note that, although its relative error is slightly greater w.r.t the near phalanges and lesser w.r.t. phalanx 5, it leads to the worst case. As recalled for position 5, this is due to the greater angle on phalanx 1, which results in the estimated force being always larger on phalanx 1 w.r.t. phalanx 2.
We can conclude that our architecture estimates a distribution of the contact forces on the foot fascia that is slightly larger than the actual one. This can lead to unstable footholds in certain foot configurations (due to a shape of the support

TABLE III
CONFUSION MATRIX OF THE EXPERIMENTAL RESULTS.

		Estimated Position					
		Pos. 1	Pos. 2	Pos. 3	Pos. 4	Pos. 5	Pos. 6
Actual Position	Pos. 1	100%	0	0	0	0	0
	Pos. 2	87.5%	0	0	0	0	12.5%
	Pos. 3	0	0	100%	0	0	0
	Pos. 4	0	0	0	87.5%	0	12.5%
	Pos. 5	0	0	0	12.5%	12.5%	75%
	Pos. 6	0	0	0	0	0	100%

polygon smaller than the actual one, see [6]). Such error could be solved, in principle, by considering a safety factor on the estimation. In general, the proposed method was able, in the majority of cases, to correctly identify the sole contact location arising from the sliding obstacle. This allows to hint at the presence/shape of terrain objects/irregularities with a radius down to 1 cm (corresponding to the least height of the sliding obstacle supports, i.e. 7 mm).

VI. CONCLUSION AND FUTURE WORK

We presented a perception system for robotic adaptive feet, exploiting their intrinsic capability of conforming to the environment. We showed that the use of a perception layer realized via IMU sensorization allows to i) reconstruct the shape of the foot, and thus visualize several characteristics of the ground beneath, and also to ii) obtain an estimate of the contact force distribution. The force reconstruction problem has been theoretically formalized and analyzed on the Sagittal plane. Then, theoretical results were experimentally validated in a simplified scenario, showing the feasibility of the method. Nevertheless, it is possible to appreciate some error in the reconstruction, the effect of which on walking stability still remains to be studied. Future work will be devoted in using this estimation to infer properties of a more interesting ground model, with non-zero friction, multiple contact on the foot sole and/or partial contacts with flat obstacles. We plan also to validate our approach in an actual walking robot, and to carry tests in dynamic cases. Finally, we aim to relax/remove hypothesis H-1, so to model more realistic locomotion interactions. Promising ways to accomplish this are the use of numerical optimization methods, or of particle filters (as e.g. in [10]).

REFERENCES

[1] D. Torricelli, J. Gonzalez, M. Weckx, R. Jiménez-Fabián, B. Vanderborght, M. Sartori, S. Dosen, D. Farina, D. Lefeber, and J. L. Pons, "Human-like compliant locomotion: state of the art of robotic implementations." *Bioinspiration & biomimetics*, vol. 5, no. 11, 2016.

[2] M. Hutter, C. Gehring, D. Jud, A. Lauber, C. D. Bellicoso, V. Tsounis, J. Hwangbo, K. Bodie, P. Fankhauser, M. Bloesch *et al.*, "Anymal-a highly mobile and dynamic quadrupedal robot," in *2016 IEEE/RSJ International Conference on Intelligent Robots and Systems (IROS)*. IEEE, 2016, pp. 38–44.

[3] A. Spröwitz, A. Tuleu, M. Vespignani, M. Ajallooeian, E. Badri, and A. J. Ijspeert, "Towards dynamic trot gait locomotion: design, control, and experiments with cheetah-cub, a compliant quadruped robot." *Int J Rob Res.*, vol. 8, no. 32, 2013.

[4] N. G. Tsagarakis, Z. Li, J. Saglia, and D. G. Caldwell, "The design of the lower body of the compliant humanoid robot "ccub"," in *2011 IEEE International Conference on Robotics and Automation*. IEEE, 2011, pp. 2035–2040.

[5] H.-j. Kang, K. Hashimoto, H. Kondo, K. Hattori, K. Nishikawa, Y. Hama, H.-o. Lim, A. Takanishi, K. Suga, and K. Kato, "Realization of biped walking on uneven terrain by new foot mechanism capable of detecting ground surface," in *2010 IEEE International Conference on Robotics and Automation*. IEEE, 2010, pp. 5167–5172.

[6] C. Piazza, C. Della Santina, G. M. Gasparri, M. G. Catalano, G. Grioli, M. Garabini, and A. Bicchi, "Toward an adaptive foot for natural walking," in *2016 IEEE-RAS 16th International Conference on Humanoid Robots (Humanoids)*. IEEE, 2016, pp. 1204–1210.

[7] S. Hauser, M. Mutlu, P. Banzet, and A. Ijspeert, "Compliant universal grippers as adaptive feet in legged robots," *Advanced Robotics*, vol. 32, no. 15, pp. 825–836, 2018.

[8] R. Käslin, H. Kolvenbach, L. Paez, K. Lika, and M. Hutter, "Towards a passive adaptive planar foot with ground orientation and contact force sensing for legged robots," in *2018 IEEE/RSJ International Conference on Intelligent Robots and Systems (IROS)*. IEEE, 2018.

[9] L. Paez, K. Melo, R. Thandiackal, and A. J. Ijspeert, "Adaptive compliant foot design for salamander robots," in *2019 2nd IEEE International Conference on Soft Robotics (RoboSoft)*. IEEE, 2019.

[10] L. Manuelli and R. Tedrake, "Localizing external contact using proprioceptive sensors: The contact particle filter," in *2016 IEEE/RSJ International Conference on Intelligent Robots and Systems (IROS)*. IEEE, 2016, pp. 5062–5069.

[11] D. Kim, Y. Zhao, G. Thomas, B. R. Fernandez, and L. Sentis, "Stabilizing series-elastic point-foot bipeds using whole-body operational space control," *IEEE Transactions on Robotics*, vol. 32, no. 6, pp. 1362–1379, 2016.

[12] M. Vukobratović and B. Borovac, "Zero-moment point: thirty five years of its life," *International Journal of Humanoid Robotics*, vol. 1, no. 01, pp. 157–173, 2004.

[13] J. R. Guadarrama-Olvera, F. Bergner, E. Dean, and G. Cheng, "Enhancing biped locomotion on unknown terrain using tactile feedback," in *2018 IEEE-RAS 18th International Conference on Humanoid Robots (Humanoids)*. IEEE, 2018, pp. 1–9.

[14] B. Belzile and L. Birglen, "Stiffness analysis of underactuated fingers and its application to proprioceptive tactile sensing," *IEEE/ASME Transactions on Mechatronics*, vol. 21, no. 6, pp. 2672–2681, 2016.

[15] C. Della Santina, C. Piazza, G. Santaera, G. Grioli, M. Catalano, and A. Bicchi, "Estimating contact forces from postural measures in a class of under-actuated robotic hands," in *2017 IEEE/RSJ International Conference on Intelligent Robots and Systems (IROS)*. IEEE, 2017.

[16] R. Putz and R. Pabst, *Sobotta-Atlas of Human Anatomy: Head, Neck, Upper Limb, Thorax, Abdomen, Pelvis, Lower Limb.*, 2006.

[17] M. Duarte and V. M. Zatsiorsky, "Patterns of center of pressure migration during prolonged unconstrained standing," *Motor control*, vol. 3, no. 1, pp. 12–27, 1999.

[18] J. Perry and J. Burnfield, "Gait analysis: normal and pathological function. new jersey: Slack," 1992.

[19] C. Della Santina, C. Piazza, G. Grioli, M. G. Catalano, and A. Bicchi, "Toward dexterous manipulation with augmented adaptive synergies: The pisa/iit softhand 2," *IEEE Transactions on Robotics*, no. 99, pp. 1–16, 2018.

[20] C. Della Santina, C. Piazza, G. M. Gasparri, M. Bonilla, M. G. Catalano, G. Grioli, M. Garabini, and A. Bicchi, "The quest for natural machine motion: An open platform to fast-prototyping articulated soft robots," *IEEE Robotics & Automation Magazine*, vol. 24, no. 1, 2017.

[21] D. F. Wilkes, "Rolamite-a new mechanical design concept," 1967.